Model Predictive Control-based Energy Management Strategy for a Series Hybrid Electric Tracked Vehicle

Hong Wang, Yanjun Huang, Amir Khajepour, Qiang Song

***Abstract*—The series hybrid electric tracked bulldozer (HETB)'s fuel economy heavily depends on its energy management strategy. This paper presents a model predictive controller (MPC) to solve the energy management problem in an HETB for the first time. A real typical working condition of the HETB is utilized to develop the MPC. The results are compared to two other strategies: a rule-based strategy and a dynamic programming (DP) based one. The latter is a global optimization approach used as a benchmark. The effect of the MPC's parameters (*e.g.* length of prediction horizon) is also studied. The comparison results demonstrate that the proposed approach has approximately a 6% improvement in fuel economy over the rule-based one, and it can achieve over 98% of the fuel optimality of DP in typical working conditions. To show the advantage of the proposed MPC and its robustness under large disturbances, 40% white noise has been added to the typical working condition. Simulation results show that an 8% improvement in fuel economy is obtained by the proposed approach compared to the rule-based one.**

***Index Terms*—Series hybrid electric tracked bulldozer, Energy management strategy, Model predictive control, Rule-based, Dynamic programming, Robustness**

I. Introduction

Construction vehicles, such as bulldozers, play a significant role in modern society. The increasing reliance on construction vehicles brings serious adverse impacts such as unsustainable energy use and poor air quality. Recently, hybrid electric construction vehicles have appeared. Caterpillar produced the first hybrid electric tracked bulldozer, D7E, in March 2008. Compared to traditional models, D7E's CO and NO_x emissions were reduced by approximately 10 and 20 percent, respectively. The D7E model can improve fuel economy by 25%. In this paper, a new HETB composed of an engine-generator, two drive motors, and an ultracapacitor pack is put forward. The powertrain topology of the HETB is shown in Fig.1. This HETB uses an integrated controller to manipulate two separate motors on the two sides. The added electric motors and ultracapacitors provide more flexibility to meet power demands and achieve minimal fuel consumption [1]. The performance or fuel economy of the HETB is heavily dependent on its energy management strategy, which uses a supervisory controller that can coordinate the energy flow between different energy sources and enhance the overall efficiency of the powertrain [2].

Recently, numerous energy management strategies have been reported and applied to hybrid electric vehicles (HEVs) [3], [4], [5], [6], and these strategies can be divided into four classes [7]. The first type refers to the numerical optimization method, where the entire or partial drive cycle is required and the global or local optima is found numerically; this type includes the DP [8],[9],[10], MPC [11],[12] and stochastic DP [13]. DP provides a globally optimal solution and is mainly employed as a good benchmark for optimality comparison [14]. In the literature [6], authors firstly propose a novel correctional DP-based energy management strategy that takes characteristics of the drive cycle and hybrid powertrain into consideration to realize the significant improvement of fuel economy and at the same time to ensure drivability during slope conditions. The second class represents the analytical optimization method including Pontryagin's minimum principle and the Hamilton-Jacobi-Bellman equation [15]. The third type is the equivalent consumption minimization strategy (ECMS) [16], which decides the optimal power split ratio between different energy sources at each step [17],[18]. Furthermore, the ECMS method does not require future driving information as it solves an instantaneous optimization problem. Given a proper equivalent factor, ECMS could potentially achieve sub-optimal fuel economy [19]. Nevertheless, it is nontrivial to tune the equivalent factor, and ECMS cannot produce globally optimal performances. ECMS is able to adjust the factor via an adaptive ECMS as long as the future driving information can be identified online to achieve better fuel economy [20], [21]. The fourth category employs fuzzy logic, heuristic rules, and neural networks for energy management strategy design [22], [23].

H. Wang is with the Mechanical and Mechatronics Engineering Department, University of Waterloo, Waterloo, ON. N2L 3G1, Canada and also with the National Engineering Laboratory for Electric Vehicles, Beijing Institute of Technology, Beijing, 100081, China (e-mail: h492wang@uwaterloo.ca).

Y. Huang and A. Khajepour are with the Mechanical and Mechatronics Engineering Department, University of Waterloo, Waterloo, ON. N2L 3G1, Canada (e-mail:y269huan@uwaterloo.ca, a.khajepour@uwaterloo.ca).

Q. Song is with the National Engineering Laboratory for Electric Vehicles, Beijing Institute of Technology, Beijing, 100081, China (e-mail:songqiang@bit.edu.cn).

Nomenclature

F_E	external travel resistance, N	h_p	bulldozer average cutting depth, m
F_T	operating resistance ,N	μ_1	friction coefficient among soil particles
F_c	compaction resistance, N	μ_2	friction coefficient between the soil and bulldozing plate
F_b	bulldozing resistance, N	Vol	the soil volume in front of the bulldozing plate, m
G	vehicle's weight, N	θ	Slope, °
b	width of the track. m	k_s	soil loose degree coefficient
L'	length of the track. m	k_y	cutting force per unit area when the plate is penetrated into the soil, MPa
c	soil cohesion coefficient, KPa	k_m	soil fullness degree coefficient
Ψ	soil internal friction angle, °	α_0	natural slope angle of the soil, °
k	soil deformation modulus， KN/m^{n+2}	X	bulldozing plate worn length contacting the ground, m
n	soil deformation index	δ	cutting angle of the bulldozing plate, °
Z	track's amount of sinkage, m	N_e	speed of engine, rpm
γ	soil unit weight ,N/m^3	P_e	engine output power, kW
N_γ, N_c	soil Terzaghi coefficients of the bearing capacity	T_e	engine torque, N
F_1	cutting force, N	n_m	motor speed, rpm
F_2	pushing force of the mound ahead of the blade, N	T_m	motor output torque, N
F_3	friction resistance between the blade and ground, N	P_{uc}	output power from the ultracapacitor, kW
F_4	component of the frictional resistance in horizontal direction when the soil rises along the blade, N	P_g	generator output power, kW
B_1	bulldozer plate width, m	η_m	motor efficiency
H	bulldozer plate height, m	C	equivalent capacitance of ultracapacitor, F
k_b	cutting force per unit area, MPa	SOC	state of charge of ultracapacitor
G_t	soil weight in front of the bulldozing plate, N	SOE	state of energy of ultracapacitor

Fig.1. Configuration of the HETB.

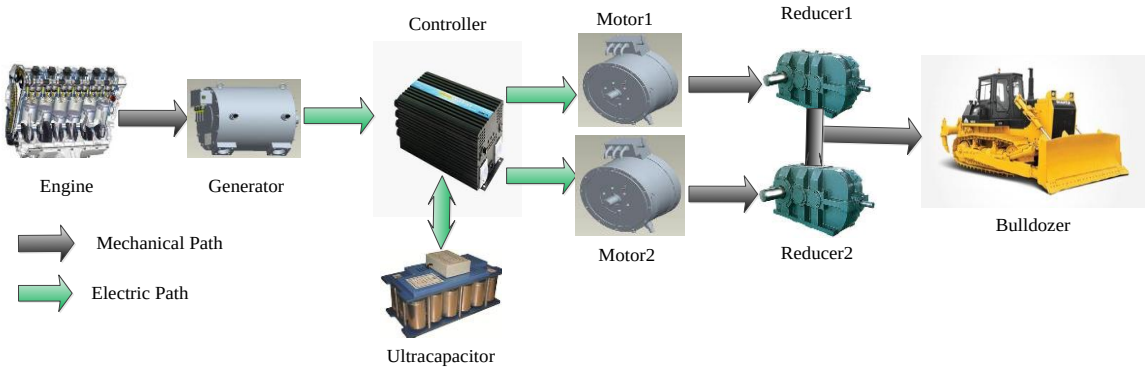

Fig.1. Configuration of the HETB.

The MPC is prevalent and widely employed in HEVs nowadays as an effective approach to deal with multivariable constrained control problems, and this strategy can be treated as a tradeoff between DP and ECMS. Currently, different kinds of MPCs are widely utilized because of their ability to deal with multivariable constrained problems and their potential for the real-time application as a receding horizon control strategy. Meanwhile, the MPC has also shown its potential for application in HEVs [24], [25], [26], [27], [28]. An MPC solves an energy management problem at every time instant by quadratic programming [29], nonlinear programming [30], Pontryagin's minimum principle [31], and stochastic DP [32]. In [33], a stochastic MPC was designed for a series HEV, where a Markov chain was used to model the future power demand. Its performance was compared to that of a prescient MPC with a fully known power demand and a frozen-time MPC using a constant power demand in the prediction horizon to demonstrate its fuel economy in a condition similar to the ideal condition (prescient MPC).

TABLE I
BASIC VEHICLE PARAMETERS

Component	Parameters	Quantity
Diesel Engine	maximum power	172kW/1800rpm
	maximum torque	1087Nm/1300rpm
Motor	maximum power	105kW
	rated power	75kW
	maximum torque	800Nm
	rated torque	500Nm
	maximum speed	6000rpm
	rated speed	1430rpm
Generator	maximum power	180kW
	rated power	175kW
	maximum torque	1010Nm
	rated torque	980Nm
	maximum speed	2200rpm
	rated speed	1700rpm
Ultracapacitor	capacity	2.4F
	voltage	600V
Vehicle	curb weight	28000kg
	track width	0.61m
	track length	3.05m
	drive wheel radius	0.46831m

Literature [34] developed an MPC for energy management with the capability to account for the uncertainty caused by traffic, destination, and weather. A modified k-nearest neighbor regressor was utilized to generate weighted samples of the upcoming drive cycle by feature matching the current state to historical states, and subsequently, an MPC was developed based on the obtained information.

In this paper, the MPC method is used to arrive at an effective energy management system for HETBs. HETBs are mainly different from road electric hybrid vehicles in working and driving conditions. Unlike HEVs, HETBs' power demands change dramatically between the soil-cutting stage and the no-load stage under a specific drive cycle. Consequently, the application of MPC strategy in HETBs is more complicated than that in HEVs. Besides, the drive cycle changes sharply according to the ground characteristic. Thus, the robustness of the HETB is more important than that of an HEV.

Three scenarios are utilized to develop the energy management controller using the MPC. The first scenario is extracted from typical working conditions of the bulldozer. The optimal solution over a typical drive cycle is obtained by achieving the maximal fuel economy and then comparing this to the results from using rule-based and DP strategies. The effect of the MPC parameters (*e.g.* length of prediction horizon) is also investigated. The comparison indicates that the proposed approach is robust to drive cycle disturbances and provide much better fuel economy over rule-based strategies. It is also indicated that the proposed MPC power management can achieve over 98% of the fuel optimality of DP without any knowledge of the changes in drive and working conditions.

The paper is organized as follows: In Section II, the HETB model is provided; the MPC is developed in Section III; the other two power management strategies are provided in the next section; the simulation results under three scenarios are compared to the rule-based strategy and the optimal solution calculated by DP in Section V; finally, comments and future work are discussed.

II. Series HETB Powertrain Model

A. System Configuration

The vehicle studied is an SD-24 tracked bulldozer from Shantui Construction Machinery Co., Ltd, and its powertrain configuration can be seen from Fig.1. The series hybrid power system is composed of a diesel engine (175kW), an ultracapacitor pack, a permanent magnet generator (175/180 kW), two motor drive systems (75/105 kW), and two tracks. A 2.4F ultracapacitor pack is utilized as an energy storage system. The integrated controller is developed and used to coordinate the power flow of the entire powertrain. Specifications of this bulldozer are given in Table I.

The HETB is modeled in SIMULINK, as shown in Fig.2. For more information regarding this model, please refer to [35].

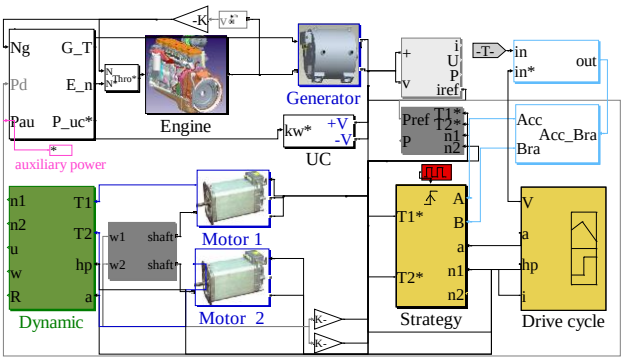

Fig.2 HETB model in SIMULINK

B. The Vehicle Model

Differing from road vehicles, the bulldozer's major external forces that are exerted on the two tracks along the heading direction include the external travel resistance F_E and the operating resistance F_T. The aerodynamic drag and the acceleration resistance are neglected since the bulldozer has a low velocity [36], [37].

The external travel resistance F_E is caused by the vertical deformation of the soil under the anterior track of the bulldozer when driving. It mainly results from the energy consumption of soil compaction and the effects of bulldozing resistance can be shown as [38]:

$$F_E = F_c + F_b \tag{1}$$

$$F_c = \frac{2b}{(n+1)k^{\frac{1}{n}}}\left(\frac{G}{2bL'}\right)^{\frac{n+1}{n}} \tag{2}$$

$$F_b = \gamma Z^2 b K_\gamma + 2bZcK_{pc} \tag{3}$$

where,

$$Z = \left(\frac{G}{2bL'k}\right)^{\frac{1}{n}} \tag{4}$$

$$K_\gamma = \left(\frac{2N_\gamma}{\tan\psi} + 1\right)\cos^2\psi \tag{5}$$

$$K_{pc} = (N_c - \tan\psi)\ \cos^2\psi \tag{6}$$

The operating resistance F_T is shown as the following [39]:

$$F_T = F_1 + F_2 + F_3 + F_4 \tag{7}$$

$$F_1 = 10^6 B_1 h_p k_b \tag{8}$$

$$F_2 = \frac{V\gamma\mu_1\cos\theta}{k_s} \tag{9}$$

$$F_3 = 10^6 B_1 X \mu_2 k_y \tag{10}$$

$$F_4 = G_t \mu_2 \cos\delta^2 \cos\theta \tag{11}$$

$$Vol = \frac{B_1(H-h_p)^2 k_m}{2\tan\alpha_0} \tag{12}$$

By combining (1) ~ (12), the vehicle's power requirements for the powertrain, P_{req}, can be formulated as:

$$P_{req} = (F_E + F_T)V \tag{13}$$

where V is the bulldozer's speed along the longitudinal direction.

C. The Engine Model

The experimental approach is adopted to model the engine, and the engine's dynamic characteristics are neglected. The engine fuel consumption is represented by a function of the mechanical power and crankshaft speed, both of which were identified from experimental data as shown in Fig. 3.

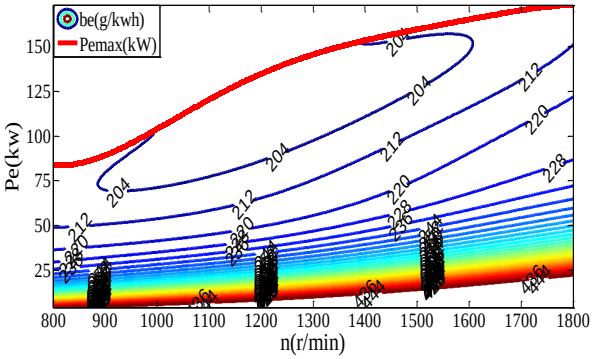

Fig.3.Fuel consumption map of the diesel engine

Assuming that engine is able to operate at the fixed speed, the fuel consumption $\dot{B}_e(g/s)$ is a function with respect to the mechanical power, P_e:

$$\dot{B}_e = \dot{B}_e(P_e) \tag{14}$$

The engine is constrained to operate within its limits:

$$\begin{aligned} N_{e,\min}(t) \le N_e(t) \le N_{e,\max}(t); \\ P_{e,\min}(t) \le P_e(t) \le P_{e,\max}(t); \\ T_{e,\min}(t) \le T_e(t) \le T_{e,\max}(t); \end{aligned} \tag{15}$$

where $N_{e,min}(t)$ and $N_{e,max}(t)$ represent the lower and upper limit of engine speed at time t, respectively; $P_{e,min}(t)$ and $P_{e,max}(t)$ are the limits of the output power, respectively; whereas, $T_{e,min}(t)$ and $T_{e,max}(t)$ are the minimum and maximum engine torque at time t, respectively.

D. The Generator and Motor Models

The generator and motor efficiency characteristics are represented by a non-linear 3-D Map with respect to torque and speed using experimental data. The generator efficiency map is provided in Fig.4, and the motor efficiency map is indicated in Fig.5. The motor efficiency η_m at the operation point (n_m, T_m) is calculated according to the following correlation:

$$\eta_m(n_m, T_m) = f(n_m, T_m) \tag{16}$$

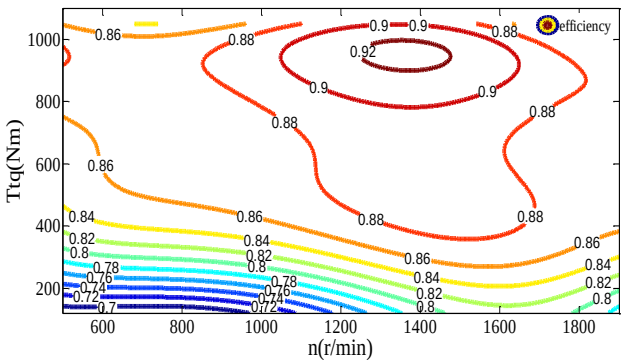

Fig.4 Generator efficiency map

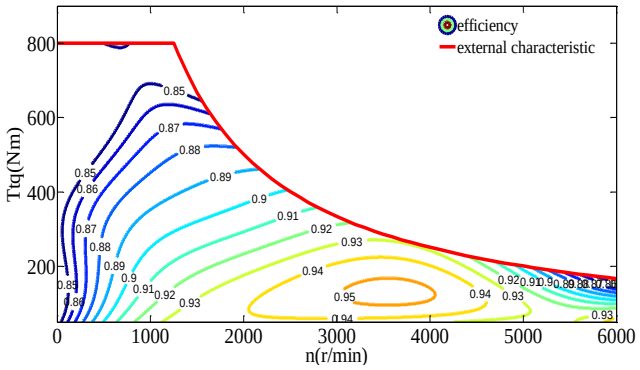

Fig.5 Motor efficiency map

E. The Ultracapacitor Model

The ultracapacitor pack is composed of several units in both parallel and series modes. Each unit can be modeled as a resistor in series with a capacitance. The resistance models the electrolyte losses, while the capacitance calculates ion accumulation. The model of the entire ultracapacitor pack can be denoted by:

$$P_{uc}(t) = V_L(t).I_{cap}(t) \tag{17}$$

$$\dot{V}_{cap}(t) = -\frac{1}{C} I_{cap}(t) \tag{18}$$

$$SOC(t) = \frac{Q(t)}{Q_{\max}} = \frac{CV_{cap}(t)}{CV_{\max}} = \frac{V_{cap}(t)}{V_{\max}} \tag{19}$$

$$SOE(t) = \frac{E(t)}{E_{cap}} = \frac{\frac{1}{2}CV_{cap}(t)^2}{\frac{1}{2}CV_{\max}{}^2} = \frac{V_{cap}(t)^2}{V_{\max}{}^2} = SOC(t)^2 \tag{20}$$

where V_L is the terminal voltage; V_{cap} is the voltage across the equivalent capacitance; V_{max} is the ultracapacitor's maximum voltage; I_{cap} is the current; Q_{max} is the maximum acceptable amount of capacity; $Q(t)$ is the amount of charge stored in the capacitance; E_{cap} is maximum energy capacity; and $E(t)$ represents the amount of energy stored in the capacitance.

The relationship among the differential of *SOE*, the maximum energy capacity, and the ultracapacitor power is shown in (21). Since the problem is modeled by the power balance equations, choosing the *SOE* as the control variable for the HETB is more natural. The dynamic equation of the *SOE* variation is shown as:

$$\dot{SOE}(t) = \begin{cases} -\frac{1}{\eta_{cap}} \frac{P_{uc}(t)}{E_{cap}} & if\ P_{uc}(t) \ge 0\ \ (disch\arg e) \\ -\eta_{cap} \frac{P_{uc}(t)}{E_{cap}} & if\ P_{uc}(t) < 0\ \ (ch\arg e) \end{cases} \tag{21}$$

where η_{cap} is the ultracapacitor's efficiency.

The power balance model for the electrical summation node is shown in Fig.6, where the relationship among the power from the genset, the electric motor, and the ultracapacitor is described as:

$$P_{uc} = P_{gen,e} + P_{req} \tag{22}$$

$$P_e = \frac{P_{gen,e}}{\eta_g} = \frac{P_{uc} - P_{req}}{\eta_g} \tag{23}$$

where P_{req} is the power requirements from the powertrain; $P_{gen,e}$ denotes the electric power from the genset; and η_g is the generator efficiency.

From (22), the following constraints on P_{uc} are derived:

$$P_{req}(t) - P_{gen,e,\max} \le P_{uc}(t) \le P_{req}(t) - P_{gen,e,\min} \tag{24}$$

Furthermore, P_{uc} and the *SOE* must be satisfied together with the physical constraints:

$$P_{uc,\min}(t) \le P_{uc}(t) \le P_{uc,\max}(t) \tag{25}$$

$$SOE_{\min} \le SOE(t) \le SOE_{\max} \tag{26}$$

where $P_{gen,e,max}$ represents the maximum electric power from the genset; $P_{gen,e,min}$ refers to the minimum power; $P_{uc,max}$ is the maximum output power of ultracapacitor; $P_{uc,min}$ is the minimum output power; SOE_{max} denotes the maximum state of energy; and SOE_{min} is the minimum state of energy.

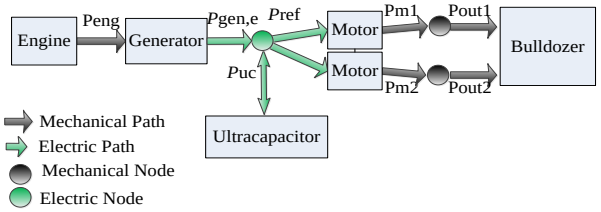

Fig.6. Power flow of the HETB.

III. MPC DEVELOPMENT FOR SERIES HETB

As an optimal control method, the MPC originated as a control technique in the chemistry industry. It is characterized by its slow dynamics, which provides enough time for optimization calculations. According to the HETB model developed in the previous section, the model predictive controller can be developed using the following equations:

$$\begin{aligned} \dot{x}_1 &= -\frac{u(t)}{E_{cap}} \\ \dot{x}_2 &= \dot{B}_e(P_e) = \dot{B}_e\left(\frac{P_{uc} - P_{req}}{\eta_g}\right) \end{aligned} \tag{27}$$

where x_1=*SOE* and x_2=B_e denotes the fuel consumption; while, u=P_{uc} represents the control input.

The vectors of states, control inputs, measured inputs, as well as the outputs are defined as:

$$x = \begin{bmatrix} SOE \\ B_e \end{bmatrix}, u = P_{uc}, v = P_{req}, y = \begin{bmatrix} SOE \\ B_e \end{bmatrix} \tag{28}$$

The linearized and discretized model of the system becomes:

$$\left.\begin{aligned} x(k+1) &= A(k)x(k) + B_u(k)u(k) + B_v(k) \\ y(k) &= C(k)x(k) \end{aligned}\right\} \tag{29}$$

In this equation,

$$A = \begin{bmatrix} 1 & 0 \\ 0 & 1 \end{bmatrix}; B_u(k) = \begin{bmatrix} -\frac{1}{E_{cap}} \\ -m_1 \end{bmatrix}; B_v(k) = \begin{bmatrix} 0 \\ m_1 * P_{ref} + m_2 \end{bmatrix}; C(k) = \begin{bmatrix} 1 & 0 \\ 0 & 1 \end{bmatrix};$$

The cost function to be minimized can be described by:

$$\begin{aligned} &\min_{u_0, u_1, \ldots u_{N-1}} J \\ &= \min_{u_0, u_1, \ldots u_{N-1}} \sum_{i=1}^{N-1} \left[w_{i+1}{}^{y} \left\| y(k+i+1|k) - y_{ref}(k+i+1|k) \right\|^2 + w_i^u \left\| u(k+i|k) \right\|^2 \right] \\ &= \min_{u_0, u_1, \ldots u_{N-1}} \sum_{i=1}^{N-1} \left[y(k+i+1|k) - y_{ref}(k+i+1|k) \right]^T Q \\ &\quad \left[y(k+i+1|k) - y_{ref}(k+i+1|k) \right] + u(k+i|k)^T R u(k+i|k) \end{aligned} \tag{30}$$

s.t.

$$\begin{aligned} y_{\min} \le y(k) \le y_{\max}, k = 0,1,\ldots N-1 \\ u_{\min} \le u(k) \le u_{\max}, k = 0,1,\ldots N-1 \end{aligned}$$

In the above equation, N is the prediction horizon length; w^y and w^u refers to the weights for the output y and control input u, respectively.

The objective function has been formulated for the energy management problem of the HETB. The main objective is to achieve optimal fuel economy by tracking the *SOE* reference value. The *SOE* reference trajectory is obtained from the dynamic programming (DP) optimization and the fuel consumption's reference trajectory is taken as zero. The constraints on the control effort involved are imposed by enforcing (24) and (25) at each time step. The state penalty Q and the input penalty R are:

$$Q = \begin{bmatrix} 1000000 & 0 \\ 0 & 1 \end{bmatrix}; R = 10$$

The objective function is transferred into a quadratic form with regard to the control input. The trajectory of future states will be obtained by the discrete model as the prediction horizon length is N [40]:

$$\begin{aligned} \underbrace{\begin{bmatrix} x(k+1) \\ x(k+2) \\ \vdots \\ x(k+N) \end{bmatrix}}_{\bar{X}} &= \underbrace{\begin{bmatrix} A \\ A^2 \\ \vdots \\ A^N \end{bmatrix}}_{S^x} x(k) + \underbrace{\begin{bmatrix} B_u & 0 & \cdots & 0 \\ AB_u & B_u & \cdots & 0 \\ \vdots & \vdots & \ddots & 0 \\ A^{N-1}B_u & A^{N-2}B_u & \ldots & B_u \end{bmatrix}}_{S^u} \underbrace{\begin{bmatrix} u(k) \\ u(k+1) \\ \vdots \\ u(k+N-1) \end{bmatrix}}_{\bar{U}} \\ &+ \underbrace{\begin{bmatrix} B_v(k) \\ B_v(k) + B_v(k+1) \\ \vdots \\ B_v(k) + B_v(k+1) + \cdots B_v(k+N-1) \end{bmatrix}}_{V} \end{aligned} \tag{31}$$

$$\underbrace{\begin{bmatrix} y(k+1) \\ y(k+2) \\ \vdots \\ y(k+N) \end{bmatrix}}_{\bar{Y}} = \underbrace{\begin{bmatrix} C & 0 & 0 & 0 \\ 0 & C & 0 & 0 \\ 0 & 0 & \ddots & 0 \\ 0 & 0 & 0 & C \end{bmatrix}}_{C^x} \bar{X}$$

The convex quadratic objective function only with respect to the input will be obtained by inserting (31) into the original objective function shown in (30) and neglecting the constant term:

$$J(x_0, u_0) = \frac{1}{2} \bar{U}^T H \bar{U} + F^T \bar{U} \tag{32}$$

$$H = 2(C^x S^u)^T \bar{Q}(C^x S^u) + \bar{R}$$

$$F = 2(C^x S^u)^T \bar{Q}(C^x S^u - \bar{Y}_{ref})$$

s.t.

$$\bar{U} \geq \max(\bar{U}_{\min}(U), \bar{U}_{\min}(\bar{U}), \bar{U}_{\min}(X)))$$

$$\bar{U} \leq \min(\bar{U}_{\max}(U), \bar{U}_{\max}(\bar{U}), \bar{U}_{\max}(X))$$

where the Hessian matrix H is symmetric and positive or semi-positive definite and F is the gradient vector. $\bar{Q}, \bar{R}$ and $\bar{Y}_{\text{ref}}$ should be reformulated according to the prediction horizon length N based on Q, R, and Y_{ref}. The updated constraints of the increment of the control can be found by the reformulation of (32) and the constraints shown in (30). For example, the constraints of the states can be applied to $\bar{U}$ as $\bar{U}_{\max}(X)$.

The energy management problem is solved by an open source solver, qpOASES [41].The optimal control input sequence u_0, u_1, u_2 …$u_{\text{N-1}}$ is obtained from the solver qpOASES, and the first element of this trajectory u_0 is applied to the plant model of the HETB. The updated value of the state is obtained in the subsequent step. The receding control strategy is implemented by repeating this procedure during subsequent time steps. The explicit expression of the quadratic programming is not reported here for the sake of brevity.

IV. Rule-based and DP-based Energy Management Strategies

In this paper, three energy management strategies have been designed in order to study the potential fuel economy of an HETB: rule-based strategy, DP, and MPC.

A. The Rule-based strategy

Utilizing a set of rules is the most popular and easiest method of implementing supervisory control in an HEV and deciding on the power split ratio between the engine and the other energy storage system [42]. The parameters of a rule-based controller are usually obtained from the powertrain modeling and simulation, possibly by using optimization techniques. In this study, the rule-based approach is implemented as follows: the engine output power follows the power demand of the bulldozer, and the ultracapacitor acts as the auxiliary power source to supply power for the power shortage caused by the excessive load of the power demand. The *SOC* of the ultracapacitor and load power requirement determines the working point of the engine-generator, as shown in Table II.

TABLE II
Rule-based Control Strategy

Judgment	State of the UC	Power supply
$P^* < P_{e\_\max}$	Charging	$P_g = \eta_g * P_e$
$SOC < SOC_{\max}$		$P_{uc} = P_{dc} - P_g$
$P^* < P_{e\_\max}$	Not-working	$P_g = \eta_g * P_e$
$SOC \geq SOC_{\max}$		$P_{uc} = 0$
$P^* > P_{e\_\max}$	Discharging	$P_g = \eta_g * P_{e\_\max}$
$SOC > SOC_{\min}$		$P_{uc} = P_{dc} - P_g$
$P^* > P_{e\_\max}$	Not-working	$P_g = \eta_g * P_{e\_\max}$
$SOC \leq SOC_{\min}$		$P_{uc} = 0$

In this table, $P_{\text{e\_max}}$ represents the engine's maximum power; P^* refers to the target demand power; P_{dc} represents the DC bus demand electric power; P_{uc} is the ultracapacitor power; and $SOC_{\max}$ and $SOC_{\min}$ are the ultracapacitor maximum and minimum state of charge, respectively.

B. Dynamic programming

Differing from the rule-based strategy, the DP algorithm usually depends on a model to provide a provably optimal control strategy by searching all state and control grids exhaustively [43], [44]. However, the DP-based approach is not suitable for real-time application since the exact future driving information is seldom known in the real world [45]. Nonetheless, the DP-based strategy can provide a good benchmark for evaluating the optimality of other algorithms, which helps in ultimately perfecting real-time strategies [46], [47], [48].

The problem setup for the DP-based strategy requires discrete values of the control variable and a discrete-time description of the system. The procedure of DP is implemented as follows [6].

1) Problem Formulation

The state and the control variables need to be determined in order to formulate the DP. As mentioned, the state is the *SOE*. The control input refers to the output power of the ultracapacitor. The discrete-time model of the HETB can be expressed as:

$$x(k+1) = f(x(k), u(k)) \tag{33}$$

In the above equation, $u(k)$ and $x(k)$ are the control inputs and the state variables, respectively. The sampling time is chosen as 1 second.

The purpose of this optimization problem is to obtain the optimal control sequence, $u(k)$, and minimize the fuel consumption over a given drive cycle. The cost function of this optimization problem is described as follows:

$$J = \sum_{k=0}^{M-1} L(x(k), u(k)) \tag{34}$$

where, L means the instantaneous cost value and M is the time length of the specific drive cycle.

The physical constraints of state and control variables are denoted by the following inequalities to guarantee smooth/safe operation of the key components, including the engine, motor, and ultracapacitor:

$$\begin{cases} SOC_{\min} \leq SOC \leq SOC_{\max}; \\ SOE_{\min} \leq SOE \leq SOE_{\max}; \\ N_{e\_\min} \leq N_e \leq N_{e\_\max}; \\ P_{e\_\min} \leq P_e \leq P_{e\_\max}; \\ T_{e\_\min} \leq T_e \leq T_{e\_\max}; \end{cases} \tag{35}$$

Furthermore, the equality constraints are used such that the HETB can satisfy load and speed requirements at all times.

2) Implementing Dynamic Programming

The main merit of DP is that it is able to deal with the

nonlinear problem and constraints while obtaining the optimal policy. The DP problem can be described by (36) and (37):

Step M-1:

$$J^*_{M-1}(x(M-1)) = \min_{u(M-1)} \left[L(x(M-1), u(M-1)) \right] \quad (36)$$

Step k, for $0 \le k < M-1$:

$$J^*_k(x(k)) = \min_{u(k)} \left[L(x(k), u(k)) + J^*_{k+1}(x(k+1)) \right] \quad (37)$$

where $J_k^*(x(k))$ refers to the optimal accumulated cost from time step t_k to the terminal; whereas, $x(k+1)$ means the state at the $(k+1)$th stage when the control variable u_k is applied at the time step t_k according to (29).

The optimal control policy is obtained by solving the above recursive equation backwards. The minimizations are conducted subject to the equality constraints imposed by the drive cycle and the inequality constraints shown in (35).

V. Case Study

In this section, the results obtained by the aforementioned three energy management strategies are compared and discussed in three scenarios.

A. Scenario 1: Typical working condition

In this scenario, a typical working condition is used for the simulation to investigate the effect of the prediction horizon length. In Fig. 7, Velocity (km/h) is the bulldozer velocity and the depth (m) is soil-cut depth. The working stages are described as follows: 1~4-s is the traveling stage; 4~16-s is the soil-cutting stage; 16~31-s is the soil-transportation stage; 31~33-s is the unloading soil stage, and 33~50-s is the no-load stage. Fig.8 shows the power demand calculated according to the typical working condition by the equations described in Section II.

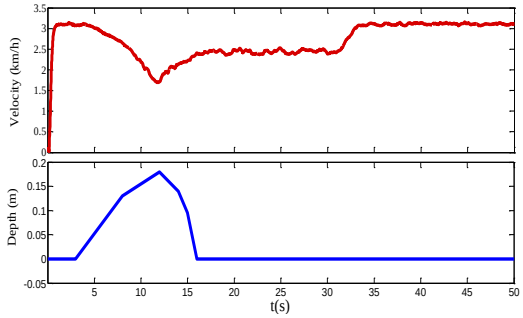

Fig.7 Typical working condition of HETB

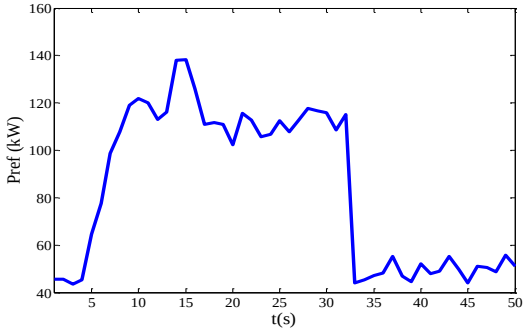

Fig.8 Power demand of the typical working condition

The most important MPC parameter that affects the solution is the length of the prediction horizon, N, which can be 2s, 4s, or 15s. Fig.9 shows the *SOE* profile corresponding to the different lengths of prediction horizons and the optimal solution obtained from the DP algorithm. It can be observed that as the prediction horizon increases, the MPC draws closer to the optimal solution. The improvement in fuel economy is provided in Table III. To compensate for the discrepancy between the initial *SOE* and final *SOE*, the correction method proposed in [13] is used such that the comparison can be performed. As seen from Table III, the fuel consumption also decreases with an increase of the receding horizon. Finally, a prediction horizon of 15s will be chosen and used in the MPC development in the following two scenarios.

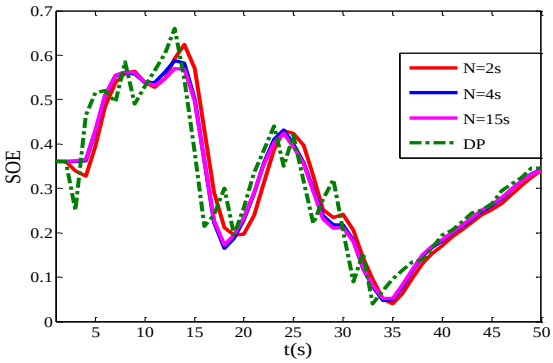

Fig.9.SOE profile with different length of prediction horizon.

Fig.10 shows the *SOE*, ultracapacitor's current, engine power, and the ultracapacitor's output power. The trajectories of the engine's power and the ultracapacitor's power demonstrate the optimal power split between two energy resources to result in minimal fuel consumption. Fuel economy achieved by the MPC algorithm is compared to the DP algorithm and the rule-based algorithm over the same working condition shown in Fig.7. As indicated in Table III, DP helps the HETB consume the minimal amount of fuel, 290g. The fuel consumption of the rule-based algorithm from the previous work is 313g, and its fuel economy is 92.6% of the optimal one. The fuel economy of the MPC algorithm is better than that of the rule-based algorithm and much closer to that of the DP algorithm. An additional 6% fuel economy is obtained by MPC algorithm over the rule-based one. The MPC can achieve 98.6% fuel optimality in relation to the optimal DP under a typical driving scenario. Although DP cannot be used in real time, analyzing its behavior can provide meaningful insight into the possible improvement of the MPC controller.

TABLE III
Fuel Consumption Comparison Under Scenario 1

Control Strategy		Fuel Consumption (g)	Fuel Economy (%)
DP		290	100
Rule-based		313	92.6
MPC	N=2	295.4	98.1
	N=4	294.6	98.4
	N=15	294	98.6

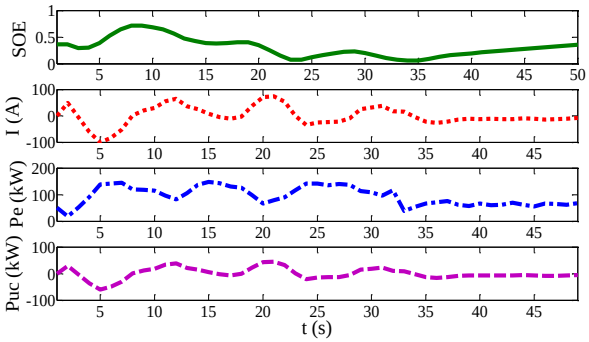

Fig.10. MPC results under scenarios 1

B. *Scenario 2: The Working Condition under Disturbances*

In order to verify the robustness of the proposed MPC strategy, a disturbance of 40% is added to the typical working condition as shown in Fig.11.

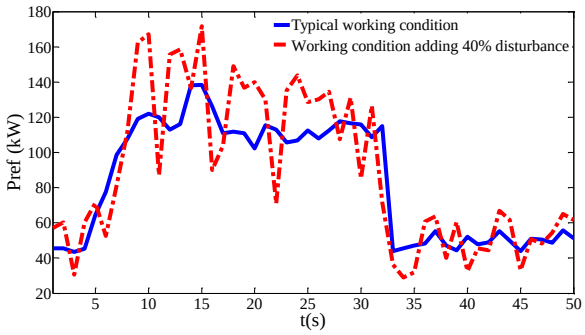

Fig.11. Power demand comparison under scenario 2

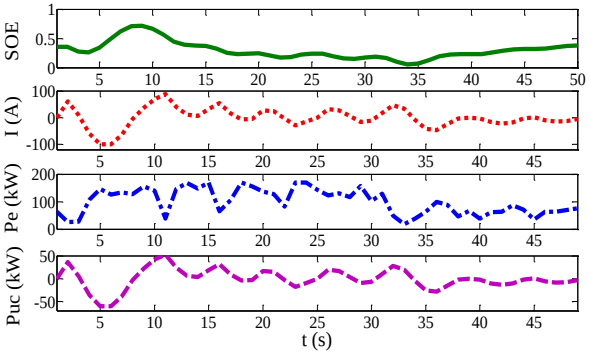

Fig.12. MPC results under scenario 2

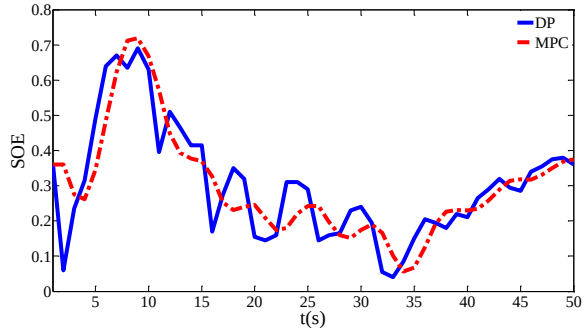

Fig.13. SOE profile comparison under scenario 2

The results of the system *SOE*, ultracapacitor's current, engine power, and input P_{uc} are presented in Fig.12. Fig. 13 shows the comparison of the *SOE* between the MPC and the DP under Scenario 2. The fuel consumption of the three energy management strategies is shown in Table IV. The MPC algorithm can achieve 98.9% fuel optimality with respect to the DP benchmark under scenario 2; whereas, the rule-based power management can only achieve 91%. The MPC strategy can obtain an additional 8% fuel economy improvement over that of the rule-based strategy. We can conclude that the MPC strategy is more effective when the working condition is not fully known.

TABLE IV
FUEL CONSUMPTION COMPARISON IN SCENARIO 2

Control Strategy	Fuel Consumption (g)	Fuel Economy (%)
DP	304.7	100
Rule-based	334.8	91
MPC	308	98.9

C. *Scenario 3: The Combined Working Condition*

Although the working condition is preset, there would be uncertainties or disturbances in real applications where the real working condition would distribute around the typical, preset working condition. Therefore, a combined working condition with a 40% disturbance is used to evaluate the MPC's robustness, as shown in Fig.14. The same MPC power management strategy is used for the disturbed combined working conditions.

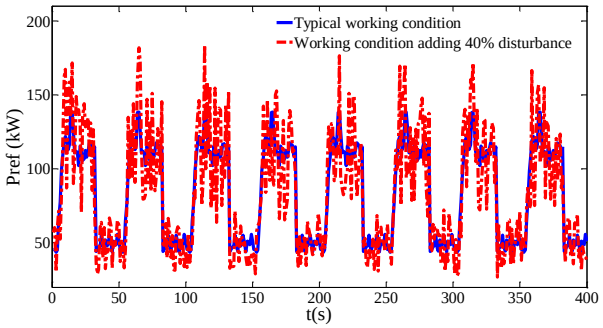

Fig.14. Power demand comparison under scenario 3

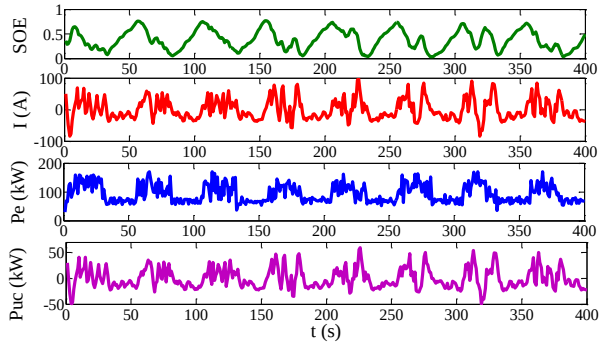

Fig.15. Power demand comparison under scenario 3

TABLE V
FUEL CONSUMPTION COMPARISON IN SCENARIO 3

Control Strategy	Fuel Consumption (g)	Fuel Economy (%)
DP	2259.5	100
Rule-based	2583.6	87.5
MPC	2376.9	95

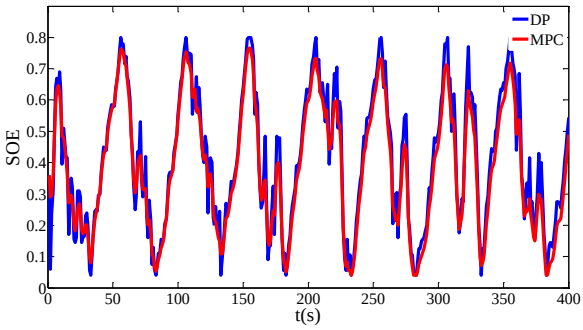

Fig.16. SOE profile comparison under scenario 3

The results of the system *SOE*, ultracapacitor's current, engine power, and input P_{uc} are presented in Fig.15. Fig. 16 shows the comparison of the *SOE* between the MPC and the DP under scenario 3. The fuel consumption comparison is shown in Table V. The DP-based control strategy with the actual working condition is used to evaluate the MPC and rule-based performances in the presence of drive cycle disturbances. It can be seen from Table V that the MPC algorithm can achieve 95% fuel optimality with respect to the DP benchmark under scenario 3 while the rule-based power management can only achieve 87.5%. An additional 8% fuel economy improvement is obtained from the MPC algorithm over that of the rule-based strategy.

The conclusion can be drawn that even under disturbed conditions, the MPC can work very well in spite of using the typical working condition for its prediction. One simulation step has the calculation time of mere milliseconds, so this proposed MPC can be used in real time. All results demonstrate that the proposed MPC is robust and applicable.

VI. Conclusion

The application of the model predictive energy management strategy of a series HETB was presented in this study. In order to develop the MPC strategy, the structure and modeling of the HETB were discussed, and the effect of the most important MPC parameters was investigated after implementation of the proposed strategy.

This paper also presented a comparative study between the MPC and two other strategies: 1) rule-based control strategy; 2) DP algorithm for minimizing fuel consumption. The structure and modeling of the HETB were developed first. Using this model, the formulations of three energy management strategies were presented. Simulation results showed that under the typical working condition, the fuel economy achieved with the MPC is 6% better than that achieved by the rule-based algorithm. The proposed MPC power management also demonstrated that it can achieve 98% fuel optimality with respect to the DP benchmark in the typical working condition.

In order to verify the advantage of the MPC strategy under large disturbances, a 40% white noise was added to the typical working condition. Simulation results demonstrated that the MPC strategy can obtain an additional 8% fuel economy improvement over that of the rule-based strategy under disturbed scenarios. This shows the robustness of the proposed energy management for large disturbances.

Further simulation and experimental investigations are underway to test and verify these quantitative results. Future work will focus on real-world cases to evaluate the proposed power management strategy and to make it more robust under all working and driving conditions.

References

[1] Xiaosong Hu, Nikolce Murgovski, Lars Johannesson, and Bo Egardt. "Energy efficiency analysis of a series plug-in hybrid electric bus with different energy management strategies and battery sizes." *Applied Energy* 111(2013):1001-1009.

[2] H. A. Borhan, A. Vahidi, A. M. Phillips, M. L. Kuang, and I. V. Kolmanovsky, "Predictive energy management of a power-split hybrid electric vehicle," in *Proc. Amer. Control Conf. (ACC)*, Jun. 2009, pp.3970-3976.

[3] Song, Ziyou, et al. "Energy management strategies comparison for electric vehicles with hybrid energy storage system." *Applied Energy* 134 (2014): 321-331.

[4] Li, Liang, et al. "Driving-behavior-aware stochastic model predictive control for plug-in hybrid electric buses." *Applied Energy* 162 (2016): 868-879.

[5] Kamil Çag˘atay Bayindir, et al, "A comprehensive overview of hybrid electric vehicle: powertrain configurations, powertrain control techniques and electric control units," *Energy Conversion and Management* 52 (2011) 1305–1313, 2011.

[6] Li, Liang, et al. "Correctional DP-based energy management strategy of plug-in hybrid electric bus for city-bus route." *Vehicular Technology, IEEE Transaction on* 64.7 (2015): 2792-2803.

[7] Zhang, Shuo, Rui Xiong, and Jiayi Cao. "Battery durability and longevity based power management for plug-in hybrid electric vehicle with hybrid energy storage system." *Applied Energy* 179 (2016): 316-328.

[8] R. Wang, and S. M. Lukic, "Dynamic programming technique in hybrid electric vehicle optimization," *Electric Vehicle Conference (IEVC), 2012 IEEE International*, Mar. 2012, pp. 1-8.

[9] J. Liu and H. Peng, "Modeling and control of a power-split hybrid vehicle," *IEEE Trans. Control Syst. Technol.*, vol. 16, no. 6, pp. 1242–1251, Nov. 2008.

[10] K. Ç. Bayindir, M. A. Gözüküçük, and A. Teke, "A comprehensive overview of hybrid electric vehicle: Powertrain configurations, powertrain control techniques and electronic control units," *Energy Convers. Manage.* , vol. 52, no. 2, pp. 1305–1313, Feb. 2011.

[11] C. Sun, X.S. Hu, S. J. Moura, and F.C. Sun, "Velocity predictors for predictive energy management in hybrid electric vehicles," *IEEE, Trans. Contr. Syst. Technol.*, vol.23, pp. 1197-1203, May 2015.

[12] T. Qu, H.Chen, D. P. Cao, H. Y. Guo, and B. Gao, "Switching-based stochastic model predictive control approach for modeling driver steering skill," *IEEE, Trans. on Intelligent Transportation Systems*, vol. 16, pp. 365-375, Feb. 2015.

[13] C. Vagg, S. Akehurst, C. J. Brace, and L. Ash, "Stochastic dynamic programming in the real-world control of hybrid electric vehicles," *IEEE, Trans. Contr. Syst. Technol.*, vol. PP, pp. 1-14, Nov. 2015.

[14] Zheng, Y., Eben Li, S., Wang, J., Cao, D., & Li, K. "Stability and scalability of homogeneous vehicular platoon: Study on the influence of information flow topologies," *IEEE Transactions on Intelligent Transportation Systems*, vol. 17, pp. 14-26, DEC. 2015.

[15] Zhang, Shuo, Rui Xiong, and Chengning Zhang. "Pontryagin's Minimum Principle-based power management of a dual-motor-driven electric bus." *Applied Energy* 159 (2015): 370-380.

[16] Sun, Chao, Fengchun Sun, and Hongwen He. "Investigating adaptive-ECMS with velocity forecast ability for hybrid electric vehicles." *Applied Energy* (2016).

[17] L. Serrao, S. Onori, and G. Rizzoni, "ECMS as a realization of Pontryagin's minimum principle for HEV control," in *Proc. Amer. Control Conf. (ACC)*, Jun. 2009, pp. 3964–3969.

[18] N. Kim, S. Cha, and H. Peng, “Optimal control of hybrid electric vehicles based on Pontryagin’s minimum principle,” IEEE Trans. *Control Syst. Technol.*, vol. 19, no. 5, pp. 1279–1287, Sep. 2011.

[19] P. Pisu, and G. Rizzoni, “A comparative study of supervisory control strategies for hybrid electric vehicles,” *IEEE Trans. Control Syst. Technol.*, vol. 15, no. 3, pp. 506–518, May 2007.

[20] C. Musardo, G. Rizzoni, Y. Guezennec, and B. Staccia, “A-ECMS: An adaptive algorithm for hybrid electric vehicle energy management,” *Eur. J. Control*, vol. 11, nos. 4–5, pp. 509–524, 2005.

[21] B. Gu and G. Rizzoni, “An adaptive algorithm for hybrid electric vehicle energy management based on driving pattern recognition,” in *Proc. ASME Int. Mech. Eng. Congr. Expo*., Jan. 2006, pp. 249–258.

[22] B. M. Baumann, G. N. Washington, B. C. Glenn, and G. Rizzoni, “Mechatronic design and control of hybrid electric vehicles,” *IEEE/ASME Trans. Mechatron.*, vol. 5, pp. 58-72, 2000.

[23] N. Schouten, M. Salman, and N. Kheir, “Fuzzy logic control for parallel hybrid vehicles,” *IEEE, Trans. Contr. Syst. Technol.*, vol. 10, pp. 460-468, May 2002.

[24] Giorgetti, N., Ripaccioli, G., Bemporad, A., Kolmanovsky, I.V., Hrovat, D.: Hybrid Model Predictive Control of Direct Injection Stratified Charge Engines. *IEEE/ASME Transactions on Mechatronics* 11(5), 499–506 (2006)

[25] Bender, F., Kaszynski, M., and Sawodny, O., “Drive cycle prediction and energy management optimization for hybrid hydraulic vehicles.” *Vehicular Technology, IEEE Transactions on*, 62(8), 3581-3592.

[26] Hu, Xiaosong, Yuan Zou, and Yalian Yang. "Greener plug-in hybrid electric vehicles incorporating renewable energy and rapid system optimization."Energy 111 (2016): 971-980.

[27] Castaings, Ali, et al. "Comparison of energy management strategies of a battery/supercapacitors system for electric vehicle under real-time constraints." *Applied Energy* 163 (2016): 190-200.

[28] Chen, Zeyu, et al. "An on-line predictive energy management strategy for plug-in hybrid electric vehicles to counter the uncertain prediction of the driving cycle." *Applied Energy* (2016).

[29] D. Rotenberg, A. Vahidi, and I. Kolmanovsky, “Ultracapacitor assisted powertrains: Modeling, control, sizing, and the impact on fuel economy,” *IEEE Trans. Control Syst. Technol.*, vol. 19, no. 3, pp. 576–589, May 2011.

[30] H. Borhan, A. Vahidi, A. M. Phillips, M. L. Kuang, I. V. Kolmanovsky, and S. Di Cairano, “MPC-based energy management of a power-split hybrid electric vehicle,” *IEEE Trans. Control Syst. Technol.*, vol. 20, no. 3, pp. 593–603, May 2012.

[31] V. Ngo, T. Hofman, M. Steinbuch, and A. Serrarens, “Predictive gear shift control for a parallel hybrid electric vehicle,” in *Proc. IEEE Veh. Power Propuls. Conf. (VPPC)*, Sep. 2011, pp. 1–6.

[32] Li, Liang, et al. "Application-Oriented Stochastic Energy Management for Plug-in Hybrid Electric Bus With AMT." *Vehicular Technology, IEEE Transactions on* 65.6 (2016): 4459-4470.

[33] Ripaccioli, G., Bernardini, D., Di Cairano, S., Bemporad, A., and Kolmanovsky, I. V., “A stochastic model predictive control approach for series hybrid electric vehicle power management.” *In American Control Conference (ACC)*, 2010 (pp. 5844-5849). IEEE.

[34] Díaz-González, Francisco, et al. "Energy management of flywheel-based energy storage device for wind power smoothing." *Applied Energy* 110 (2013): 207-219.

[35] H. Wang, Q. Song, S. B. Wang and P. Zeng, “Dynamic Modeling and Control Strategy Optimization for a Hybrid Electric Tracked Vehicle,” *Math. Probl. Eng.*, vol. 2015, doi:10.1155/2015/251906.

[36] K.K.Malay. “Prediction of track force in skid-steering of military tracked vehicle,” *Journal of TerraMechanics*, 24(1):75-86, 1987.

[37] Bekker M G. Off-Road Locomotion. The Univ. of Michigan Press, Ann Arbor, Michigan, 1960.

[38] Zhang, C. G., Zeng, K. H., Zhao, J. H, “Analytical solutions of critical load and Terzaghi’s ultimate baring Capacity for Unsaturated Soil,” *Journal of Tongji university (natural science)*, vol. 38, pp. 1736-1739, 2010.

[39] H. Wang, Q. Sun, F. C., and P. Zeng. “Parameters matching and simulation on a hybrid power system for electric bulldozer,” *Applied Mechanics and Materials*. 2012: 2137-2142.

[40] Y.J. Huang, A. Khajepour, F.Bagheri, and M.Bahrami, “Modelling and optimal energy-saving control of automotive air-conditioning and refrigeration systems,” *Proceeding of the Institution of Mechanical Engineering, Part D: Journal of Automobile Engineering*, March 23, 2016.

[41] Ferreau H J, Kirches C, Potschka A, et al, “qpOASES: A parametric active-set algorithm for quadratic programming,” *Mathematical Programming Computation*, 2014, 6(4): 327-363.

[42] X.Hu, L. Johannesson, N. Murgovski, and B. Egardt. "Longevity-conscious dimensioning and power management of the hybrid energy storage system in a fuel cell hybrid electric bus." *Applied Energy*, 137(2015): 913–924.

[43] He, Hongwen, et al. "Energy management strategy research on a hybrid power system by hardware-in-loop experiments." *Applied Energy* 112 (2013): 1311-1317.

[44] Wang, X. M., He, H. W., Sun, F. C., Zhang, J. L, “Application study on the dynamic programming algorithm for energy management of plug-in hybrid electric vehicles,” *Energies*, vol.8, pp. 3225-3244, 2015.

[45] S. Kermani, S. Delprat, T. M. Guerra, R. Trigui, B. Jeanneret, “Predictive energy management for hybrid vehicle,” *Control Eng. Pract.* , vol. 20, pp. 408-420, Apr. 2012.

[46] J. Ribau, R. Viegas, A. Angelino, A. Moutinho, and C. Sliva, “A new offline optimization approach for designing a fuel cell hybrid bus,” *Trans. Res. Part C: Emerg. Technol*., vol. 42, pp. 14-25, May 2014.

[47] H. W. He, H. L. Tang, and X. M. Wang, “Global optimal energy management strategy research for a plug-in series-parallel hybrid electric bus by using dynamic programming,” *Math. Probl. Eng.*, vol. 2013, doi:10.1155/2013/708261.

[48] L. Lai, and M. Ehsani, “Dynamic programming optimized constrained engine on and off control strategy for parallel HEV,” in *Proceedings of the IEEE Vehicle Power and Propulsion Conference(VPPC)*, Beijing, China, Nov. 2012, pp.595-613.